COMSOL
CONFERENCE
2023 MUNICH

RayOptics and Mesh Adaptation for the Study of Copper Laser Welding Process Stability Using COMSOL® Application Builder

J. Daligault[1], M. Dal[1], S. Touzouirt[1], M. Sawannia[2], C. Hagenlocher[2], R. Weber[2]
1. PIMM Laboratory, Arts et Métiers Institute of Technology (Paris), CNRS, CNAM, HESAM University, 151 Boulevard de l'Hôpital, 75013 Paris, France
2. Institut für Strahlwerkzeuge (IFSW), University of Stuttgart, Pfaffenwaldring 43, 70569 Stuttgart, Germany

Abstract
A numerical model of laser welding process applied on highly optically reflective and thermally conductive materials such as copper has been developed. The latter considers multiphysical couplings of CFD, heat transfers and Phase-field representation to account for topological deformation of the liquid-gas interface. In addition, a dedicated JAVA® method has been setup thanks to COMSOL® Application Builder to implement a new coupling between Phase-field description and geometrical optics, allowing self-consistent computation of the well-known « beam trapping effect » in laser processes. Hence, heat source induced by laser-matter interaction is updated correspondingly to liquid-gas interface fluctuations. Moreover, an adaptative mesh refinement (AMR) method is considered to counteract the high numerical complexity of such a model. Numerical results are compared to x-ray measurements of keyhole dynamic formation.
Keywords: Laser Welding, Geometrical optics, Multiphysics, Application Builder.

1. Introduction

Due to its high thermal conductivity as well as a high reflectivity, copper is known to be a challenging material for laser processes such as laser welding. However, its growing interest for e-mobility applications requires a better understanding on the physical phenomena occurring during the process.

Laser welding is an assembly process involving incident irradiances in the range of $MW.cm^{-2}$. Applied to metallic material, such irradiances allow melting at the surface of the sample, thus forming a molten pool. At certain levels, local temperatures can also reach the boiling point of the material, inducing a vaporization process. By an action-reaction principle, a recoil pressure applied at the surface deforms the molten pool and a cavity known as the keyhole or vapor capillary is created. At this point, laser-matter interaction is increased due to multiple reflections inside the cavity. This phenomenon is well-known in laser welding application and is referred to as "beam-trapping" effect.

Although the process is well mastered for materials such as steel or titanium alloys, the study of highly reflective and thermally conductive materials like aluminium or copper is still of great interest. During the process, hydrodynamical instabilities of the melt pool may occur, resulting in undesirable defects such as spatters, blow-holes or pores in the resolidified weld seam. To avoid such defects, many welding strategies have been applied on copper samples. As optical reflectivity of copper is rather high at classical industrial laser wavelength (4-8%), green lasers [1] [2] [3] have been widely used for the possible increase of materials absorptivity (40% at room temperature). However, as laser powers available at those wavelengths are not yet sufficiently high (few kW) compared to powers at classical IR-lasers (above 16 kW), this strategy has not been widely applied to obtain welds of several millimetres in depth. Power modulation [4] [5] already showed interesting results to obtain welds free of defects. Heider et al. [6] obtained significant defects reduction by applying a time modulation of the laser power during copper laser welding. Other studies focus on the use of a simpler strategy based on both high laser power and high welding speed. Fetzer et al. [7] or Reinheimer et al. [8] obtained welds deep of several millimetres and free of defects on aluminium alloys sample which are also known to be highly thermally conductive and optically reflective. On copper samples, Heider et al. [9] observed the same trend by using high power lasers in the near-IR.

Based on those experimental validation, the present paper proposes a numerical study to understand the physical phenomena leading to the positive influence of both high power and welding speed during copper laser welding. The simulation takes into account the thermo-hydrodynamic of the molten pool driven by the effect of recoil pressure, surface tension and Marangoni effect. A new coupling in COMSOL Multiphysics® is proposed to accurately represent laser-matter interaction. The latter links geometrical optics (gop) and the Eulerian phase-field (pf) interface tracking method and is developed on JAVA® in COMSOL® Application Builder.

2. Numerical Model

A. Governing equations

The basis of the model is the coupling of heat transfer and fluid mechanics to represent melt pool hydrodynamics. Hence, energy (1), mass (2) and momentum (3) conservation equations are solved, in their incompressible form, considering main driving heat fluxes and forces.

$$\rho c_p^{eq}\frac{\partial T}{\partial t}+\rho c_p^{eq}\left(\vec{u}.\vec{\nabla}T\right)-\vec{\nabla}.\left(\lambda\vec{\nabla}T\right)=Q_{abs}-Q_{loss} \quad (1)$$

$$\vec{\nabla}.\vec{u}=0 \quad (2)$$

$$\rho\frac{\partial\vec{u}}{\partial t}+\rho\left(\vec{u}.\vec{\nabla}\right)\vec{u}=\vec{\nabla}.\left(-p\bar{\bar{I}}+\mu\left[\vec{\nabla}\vec{u}+\left(\vec{\nabla}\vec{u}\right)^{T}\right]\right)+\overrightarrow{F_v} \quad (3)$$

Moreover an Eulerian description of the free boundary problem is considered to describe the liquid-gas interface deformation. The Phase-field approach based on Cahn-Hilliard equations ((4) and (5)) is used to compute the phase variable ϕ allowing the representation of a two-phase flow inside a single computational domain.

$$\frac{\partial\phi}{\partial t}+\vec{u}.\vec{\nabla}\phi=\vec{\nabla}.\left(\gamma\vec{\nabla}\psi\right) \quad (4)$$

$$\psi=-\lambda\vec{\nabla}^2\phi+\frac{\lambda}{\varepsilon^2}(\phi^2-1)\phi \quad (5)$$

Classical boundary conditions at the liquid-gas interface are thus considered as volume terms using the interface function δ [m^{-1}]. Radiative and evaporative heat losses are introduced in the energy conservation equation and expressed as:

$$Q_{loss}=\left[\epsilon\sigma_{sb}(T^4-T_0^4)+\dot{m}(T)L_v\right]\delta \quad (6)$$

Convection losses are negligeable but are still taken into account through velocity computation. In the first steps of the simulation the laser-matter interaction is implemented with an analytical description (7) considering a "top-hat" distribution with a laser beam radius r_s, a power P and material absorptivity denoted as α. Once a defined threshold is reached, this analytical expression is replaced by a dedicated method described in next section.

$$Q_{abs}=\begin{cases}\alpha\dfrac{P}{\pi r_s^2} \; if\; \sqrt{x^2+y^2}\le r_s\\ 0\; else\end{cases} \quad (7)$$

The quantity $\dot{m}$ represents the ablation rate:

$$\dot{m}=(1-\beta_r)\sqrt{\frac{M}{2\pi RT}}p_{sat}(T) \quad (8)$$

$$p_{sat}(T)=p_0\exp\left[\frac{ML_v}{RT_v}\left(1-\frac{T_v}{T}\right)\right] \quad (9)$$

Driving forces namely surface tension, Marangoni effect and recoil pressure are implemented as volume forces in the momentum conservation equation:

$$\overrightarrow{F_v}=\sigma\kappa\delta\vec{n}+\frac{\partial\sigma}{\partial T}\overrightarrow{\nabla_s}T+p_{rec}(T)\delta\vec{n} \quad (10)$$

$$p_{rec}(T)=\frac{1+\beta_r}{2}p_{sat}(T) \quad (11)$$

More details on the numerical model are given in [10].

B. Eulerian-Raytracing coupling

Laser-matter interaction is taken into account through a dedicated JAVA® method developed in COMSOL® Application Builder. The main steps are described here:

- First the multiphysical problem is solved using an analytical heat source.
- Once a critical threshold $\mathbb{C}_{stop}$ (12) defined as a maximum deviation of the phase-field is reached, the multiphysical resolution is stopped and the iso-surface $\phi=0$ is extracted as an .stl file. The latter is then used to reconstruct a physical boundary inside a second component.
- A geometrical optics (gop) physic, also referred to as ray-tracing method, is solved in this second component. Laser beam is discretized with a finite set of N_r rays distributed according to a "top-hat" distribution. A specular reflection boundary condition is set at the reconstructed interface allowing the accumulation of each ray contribution (13).
- After each reflection occurred, a general extrusion ("genext"), as well as an identity mapping ("idmap"), operator is employed to get a 3-dimensionnal field representing the irradiance along the liquid-gas interface.
- Finally, the interface δ-function is used to implement the actualized irradiance as a volume boundary condition in heat transfer equation (1).

$$\mathbb{C}_{stop}:\ \max_D\left(\left|(\phi)_t-(\phi)_{t_0}\right|\right)\ge\Delta\phi \quad (12)$$

$$P_{acc}=\sum_{i=1}^{N_r}\sum_{j=1}^{N_{refl}}\alpha P_{i,j}\vec{k}_{i,j}.\vec{n} \quad (13)$$

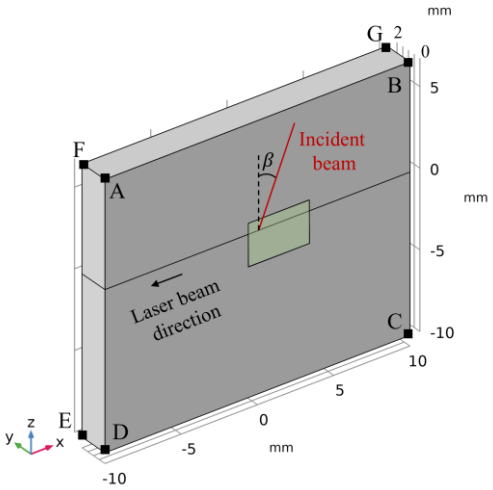

Figure 1. Computational domain and beam configuration.

The process is repeated until a laser-matter interaction time t_{pulse} is reached. By this means, the so-called beam trapping effect is taken into account self-consistently and the beam propagation is actualized according to liquid-gas interface deformation. Note that the present method could easily be transposed to a level-set interface tracking representation. Finally, laser beam divergence along its optical axis is modelled thanks to Crooker's formulation [11]. By calling x_0 and y_0 the spatial coordinates, and θ_x and θ_y the inclination angles respectively in yz- and xz-plane, one obtains the initial distribution of each ray through:

$$\mathcal{P}(x_0, y_0) = \begin{cases} 1/r_s \; if \; \sqrt{x_0^2 + y_0^2} \leq r_s \\ 0 \; else \end{cases} \quad (14)$$

$$\mathcal{P}(\theta_x, \theta_y) = \frac{2}{\pi\theta_0^2} \exp\left(-2\frac{\theta_x^2 + \theta_y^2}{\theta_0^2}\right) \quad (15)$$

In equation (15) $\theta_0 = r_s/z_R$ corresponds to the half divergence angle of the beam, where z_R is the Rayleigh length.

C. Adaptative mesh refinement

Solving the multiphysical component coupled with the ray-tracing algorithm on a domain large enough to simulate a laser welding process requires a huge amount of DOFs (degrees of freedom). To counteract the high computational cost, an adaptative mesh refinement method is added to the simulation. An initial mesh with a relatively rough mesh size h_{rough} is defined. Each time the multiphysical resolution is stopped to update beam propagation, mesh size is reduced until given target h_{AMR} where a local condition $\mathbb{C}_{AMR}$ is fulfilled.

$$\mathbb{C}_{AMR} : \left(flc2hs(T - 0.5T_m, 2\Delta T_m)\right) \vee (|z| \leq 10h_{AMR}) \quad (16)$$

Copper physical properties		Value	Ref
Heat capacity [J/kg/K]	c_p	481	[12]
Thermal conductivity [W/m/K]	λ	397	[12]
Latent heat of fusion [kJ/kg]	L_m	208.7	[12]
Latent heat of vaporization [kJ/kg]	L_v	4730	[12]
Molar mass [g/mol]	M	63.55	[12]
Melting point [K]	T_m	1357	[12]
Boiling point [K]	T_v	2868	[14]
Dynamic viscosity [mPa.s]	μ	4.38	[12]
Density [kg/m^3]	ρ	8956.5	[12]
Surface tension [N/m]	σ	1.304	[12]
Thermocapillary coefficient [mN/m/K]	$\partial\sigma/\partial T$	-0.286	[12]
Argon physical properties		**Value**	**Ref**
Heat capacity [J/kg/K]	c_p	520	[14]
Thermal conductivity [W/m/K]	λ	0.017	[14]
Molar mass [g/mol]	M	28.97	[14]
Dynamic viscosity [mPa.s]	μ	0.01	[14]
Density [kg/m^3]	ρ	1.7	[14]

Table 1. Physical properties of copper and ambient gas

The mesh is thus refined along the initial metal-gas interface and covers the entire melt pool, comprising the keyhole. This method allows a significant decrease in terms of DOFs during the transient formation of the melt pool, and therefore a reduction of the global computation time. For two simulations with identical parameters, a decrease of up to 70% computation time was obtained using the presented adaptative mesh refinement method.

D. Material properties

Copper physical properties are implemented using temperature dependent evolution presented in Table 1. Ambient gas physical properties are compiled from [12].

Indicating values of thermophysical properties of copper and ambient gas are given in Table 1.

Boundary	Fluid mecanics	Heat transfers	Phase-field
ABCD	$\vec{u}.\vec{n} = 0$	$-\vec{n}.\vec{q} = 0$	Symmetry
ADEF	$\vec{u} = V_w\vec{n}$	$-\vec{n}.\vec{q} = 0$	$\phi = \phi_0(z)$
BCHG	$p = p_0$	$-\vec{n}.\vec{q} = 0$	Outlet
ABGF	$p = p_0$	$-\vec{n}.\vec{q} = 0$	Outlet
CDEH	$\vec{u}.\vec{n} = 0$	$-\vec{n}.\vec{q} = 0$	Wetted wall $\theta_w = \pi/2$
EFGH	$\vec{u}.\vec{n} = 0$	$-\vec{n}.\vec{q} = -h(T - T_0)$	Wetted wall $\theta_w = \pi/2$

Table 2. Boundary conditions for each physic.

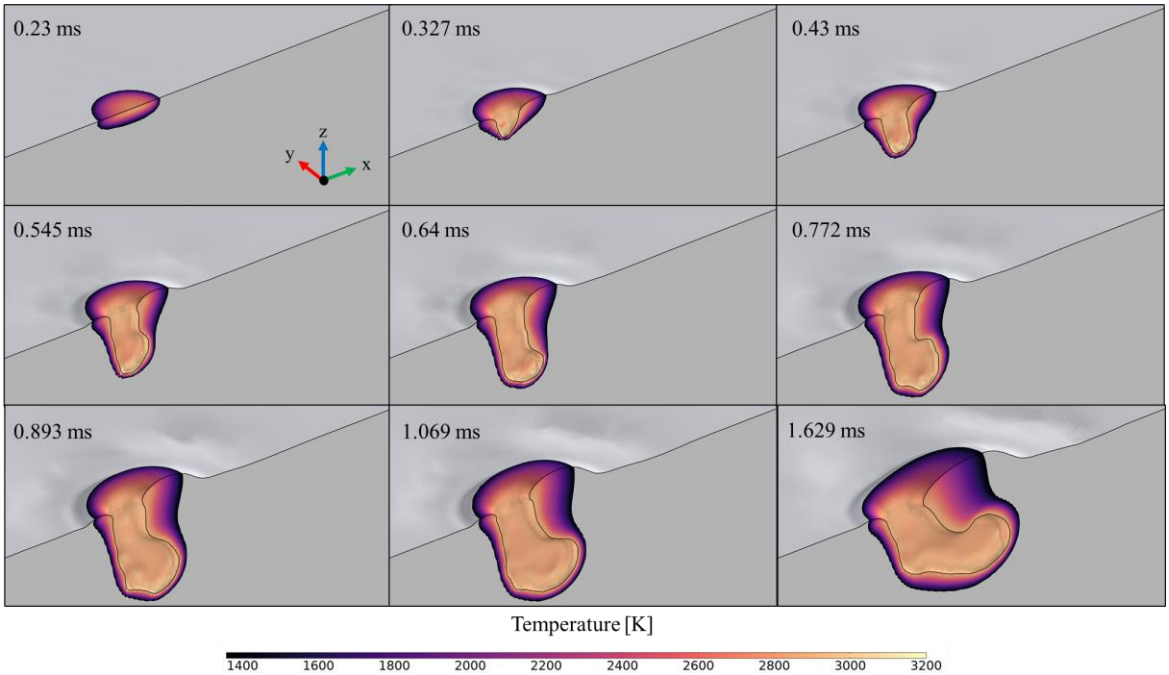

Figure 2. Molten pool and keyhole development during laser welding process.

E. Numerical setup

Since the Eulerian representation of the free interface does not impose a physical boundary between the metal and the ambient gas, a single computational domain can be used to represent a laser welding process. However, a finer mesh is only required near the metal-gas interface and around the melt pool. The frame of reference is also the frame of the laser. As a result, the laser is fixed in the geometry and the material moves beneath at a constant speed V_w. Thus, the adaptative mesh refinement is applied to a restricted region of the computational domain, shown in green in the Figure 1. To match experimental conditions, laser beam is inclined at an angle $\beta = 10°$ to ensure that no back reflections damage the optics. A pushing configuration is adopted, meaning that the laser is inclined in the opposite direction of the welding speed. Boundary conditions representing study hypotheses described above are summarized in Table 2. A symmetric condition on the xz-plane is implemented in order to reduce computation time.

The targeted mesh size h_{AMR} after refinement is set to be equal to 20 µm, after three refinement steps. In the region impacted by the AMR method, the initial mesh size h_{rough} is thus equal to $2^3 h_{AMR}$, composed of tetrahedral elements. The efficiency of the AMR method is discussed in further section. The presented results have been simulated on 18 cores at 3.67 GHz and required a simulation time around 4-5 days to simulate 2 ms of the process. Without the AMR method, a simulation with same process parameters takes around 3-4 weeks.

3. Results and discussion

The numerical model developed above is used to describe a laser welding process on a copper plate of 4 mm thickness in the y-direction. Laser beam power is set to 16 kW for a beam diameter of 400 µm at focal point and a welding speed of 30 m/min. Experimental beam is also defocused from a distance of 1.75 mm above the sample's surface, inducing an increase of the laser beam to 531.5 µm. This increase of laser beam diameter is modelled numerically through Crooker's formulation [11].

A. Keyhole development

The behaviour of the model under the process parameters described above is presented in Figure 2.

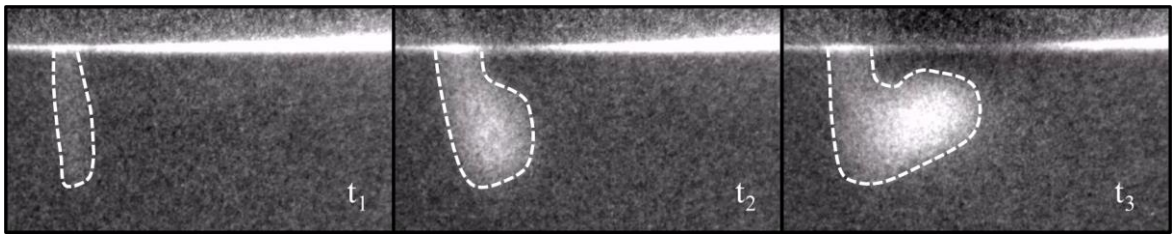

Figure 3. Transient keyhole development observed by x-ray imaging. Captured at IFSW (Stuttgart) at P = 16 kW, d = 400 µm and V_w = 10 m/min.

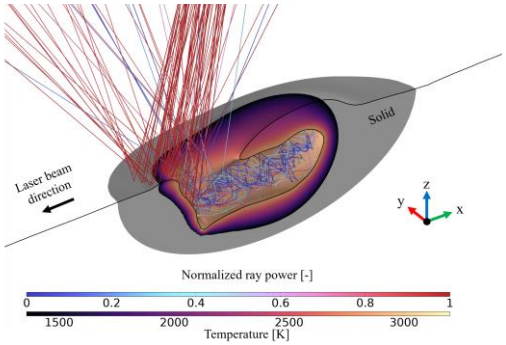

Figure 4. Beam propagation inside a reconstructed keyhole.

Soon after the start of the process, the temperature at the sample surface and under the beam rises sharply. After a few hundred µs, a molten pool is formed. As thermal diffusivity of copper is high, the dimensions of this melt pool remain close to the size of the beam. Due to the high intensities involved (MW/cm^2), the surface of the melt pool exceeds the boiling temperature after only 230 µs. A recoil pressure is then induced by vaporization and the keyhole begins to grow. In the first steps of its development, the latter adopts an inclined cylindrical shape that grows rapidly in depth. Although the weld is carried out in a pushing configuration, with the beam inclined away from its feed direction, the capillary is also inclined backward as a result of the welding speed. Around 500 µs after the beginning of the process, a bubble starts to grow at the tip of the keyhole. Due to the multiple reflections as well as the divergence of the beam, the local irradiance is no longer enough to induce a recoil pressure high enough to keep a vertical growing of the keyhole. The produced bubble grows horizontally at the back of the keyhole, while an inclined wall remains at the front.

Experimental validation has been carried out at the IFSW (Stuttgart), consisting of the in-situ observation of the capillary by means of X-ray high speed imaging. Typical measurements, made at same power and beam diameter and at a welding speed close to the numerical setup, are depicted in Figure 3. A same global behaviour is observed, with a cylindrically inclined keyhole in the first steps of the process followed by a growing of a bubble in the bottom of the capillary. This behaviour will have to be confirmed by a more complete experimental/numerical validation in future investigations, but the model already gives interesting results at this step of development.

B. Laser-matter interaction

The new coupling developed in the present paper allows an accurate and self-consistent way to model the laser-matter interaction during the process.

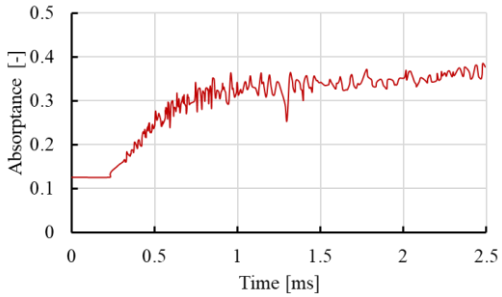

Figure 5. Global absorptance inside the keyhole during the process.

Figure 4 illustrates the propagation of the laser once the keyhole is already formed. Incident rays first interacts at the front of the keyhole, leaving a fraction α of the carried power. Then, each ray is either reflected inside of the keyhole and keeps contributing to melting the metal or reflected outside.

The absorptance, corresponding to the global fraction of the laser power that has been absorbed inside the capillary, increases rapidly (Figure 5) from the purely intrinsic absorptivity of the copper to around 2-3 times this value due to multiple reflections. Once most of the rays are reflected outwards of the keyhole or the power carried by rays inside it is no longer significant, the absorptance stabilize around 36%, meaning that 74% of the laser power does not contribute to the melting or vaporization of copper. Tracking this value might also give information on the efficiency of the process at given process parameters or welding strategies. The presented methodology allows the numerical simulation of complex fluid deformations and laser-matter interaction that is not obtainable with other classical techniques such as analytical heat sources.

C. Discussion on AMR method

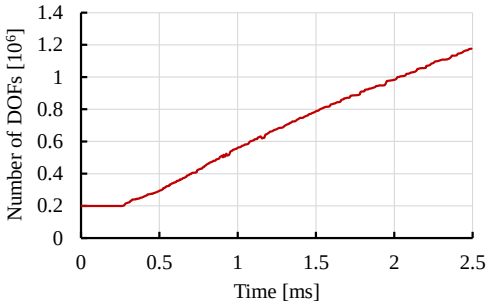

Figure 6. Evolution of the number of DOFs during the simulation.

The application of the AMR method to the current model allows a significant reduction of computation time. Compared to a model without AMR presenting a constant amount of DOFs around several millions, the first steps of our simulation consist of around 200 000 DOFs. However, as the mesh refinement is based on a thermal condition, this number of DOFs rapidly increases reaching few millions at the end of the simulation (Figure 6). Therefore, the timesaving decreases as simulation keeps running. The method will be coupled with other mesh reduction methods already found in the literature and developed on COMSOL Multiphysics® [13].

4. Conclusions

A numerical tool to understand complex physical phenomena during laser welding has been developed with a large panel of functionalities proposed by COMSOL Multiphysics®. A new coupling between geometrical optics and phase-field is proposed to model laser-matter interaction. The latter allows the representation of complex keyhole geometries as already observed experimentally. An adaptative mesh refinement method has been implemented and reduced the computation time during the transient formation of the molten pool. Even though the model presents some drawbacks, such as a possible loss of information by transferring fields between two different components, it still shows encouraging results for in-depth studies of the process. Future works will be dedicated to enhancing global convergence and coupling to use the model with different process parameters and validate numerical results with a complete experimental investigation. Then, the model will be used to study more complex process strategies such as dynamic spatial beam modulation.

Acknowledgements

The authors are grateful to Michael Sawannia, Christian Hagenlocher, Rudolf Weber and all IFSW members who contributed to the project by their work and discussions. This work was supported by Agence Nationale de la Recherche and Deutsche Forschungsgemeinschaft under the Grant ANR-19-CE08-0031 (ANR) and 431336540 (DFG).

References

[1] E. Kaiser, R. Huber, C. Stolzenburg, A. Killi, “Sputter-free and Uniform Laser Welding of Electric or Electronical Copper Contacts with a Green Laser,” *LANE*, 2014.

[2] S. Pricking, R. Huber, K. Klausmann, E. Kaiser, C. Stolzenburg, A. Killi, “High-Power CW and Long-Pulse Lasers in the Green Wavelength Regime for Copper Welding,” *SPIE*, 2016.

[3] L. Alter, A. Heider, J-P. Bergmann, “Investigations on Copper Welding Using a Frequency-Doubled Disk Laser and High Welding Speeds,” *LANE*, 2016.

[4] A. Matsunawa, J-D. Kim, N. Seto, M. Mizutani, S. Katayama, “Dynamics of Keyhole and Molten Pool in Laser Welding,” *Journal of Laser Applications*, pp. 247-254, 1998.

[5] S. Tsukamoto, I. Kawaguchi, G. Arakane, H. Honda, “Suppression of Porosity Using Pulse Modulation of Laser Power in 20 kW CO2 Laser Welding,” *ICALEO*, pp. 400-408, 2001.

[6] A. Heider, P. Stritt, A. Hess, R. Weber, T. Graf, “Process Stabilization at Welding Copper by Laser Power Modulation,” *Physics Procedia*, pp. 81-87, 2011.

[7] F. Fetzer, C. Hagenlocher, R. Weber, T. Graf, “Geometry and Stability of the Capillary During Deep-Penetration Laser Welding of AlMgSi at High Feed Rates,” *Optics & Laser Technology*, 2021.

[8] E. N. Reinheimer, F. Fetzer, R. Weber, T. Graf, “Benefit of High Feed Rates on the Process Efficiency in Laser Beam Welding,” *LANE*, pp. 718-721, 2020.

[9] A. Heider, P. Stritt, A. Hess, R. Weber, T. Graf, “High-Power Laser Sources Enable High-Quality Laser Welding of Copper,” *ICALEO*, pp. 343-348, 2014.

[10] J. Daligault, M. Dal, C. Gorny, F. Coste, R. Fabbro, “Combination of Eulerian and Ray-Tracing Approaches for Copper Laser Welding Simulation,” *Journal of Laser Applications*, 2022.

[11] P. P. Crooker, W. B. Colson, J. Blau, “Representation of a Gaussian Beam by Rays,” *American Journal of Physics*, pp. 722-727, 2006.

[12] K. C. Mills, “Recommended Values of Thermophysical Properties for Selected Commercial Alloys,” pp. 89-97, 1994.

[13] M. Courtois, M. Carin, P. Le Masson, S. Cadiou, S. Gaied, “A Method to Reduce Calculation Time in Multiphysic Modelling of Welding Processes. Application to Laser and GMAW Welding,” *COMSOL Conference,* 2019.

[14] D. R. Lide, “Handbook of Chemistry and Physics,” p. 803, 2003.